RSC Advances

PAPER

View Article Online
View Journal | View Issue

Cite this: *RSC Adv.*, 2021, **11**, 34860

Aggregation of retained helium and hydrogen in titanium beryllide $Be_{12}Ti$: a first-principles study

Yinlong Wang,†[abd] Canglong Wang,†*[bcd] Zhaocang Meng,[bcd] Jitao Liu,[bcd] Yuhong Li*[a] and Lei Yang[bcd]

Titanium beryllide, $Be_{12}Ti$, has been proposed as a prospective neutron multiplier in fusion reactors. First-principles calculations have been performed to investigate the nucleation mechanism of a He bubble in bulk $Be_{12}Ti$. Meanwhile, the influence of the presence of H atoms on the nucleation of the He bubble, *i.e.*, the synergistic effect of He and H atoms, has also been investigated. It has been found that the He bubble will initially nucleate around a monovacancy (V_{Be2}). When more He atoms have been implanted, two newly induced vacancies (V_{Be1} and V_{Be3}) could be successively observed. The nucleation of the He bubble will occur around the divacancy of $V_{Be2}V_{Be1}$ and the trivacancy of $V_{Be2}V_{Be1}V_{Be3}$. Dumbbell structures in the He bubble evolve with the number of implanted He atoms and finally disappear. The presence of H atoms will significantly influence the nucleation of the He bubble. It is interesting that some tetrahedral and octahedral structures have also been observed. The maximal number of H atoms trapped by a He bubble has been obtained. These phenomena could be further explained by the continuous shrinking of the isosurface of charge density. The present results provide a microscopic physical foundation to understand the mechanism of He and H atoms retention in neutron multiplier materials. This investigation could be helpful for the design and fabrication of more promising beryllides which could withstand a severe external environment.

Received 19th September 2021
Accepted 1st October 2021

DOI: 10.1039/d1ra07023a

rsc.li/rsc-advances

1 Introduction

As promising neutron multiplier materials, beryllium (Be) and beryllium intermetallic compounds (*e.g.*, $Be_{12}Ti$) have potential applications in accelerators of boron neutron capture therapy (BNCT)[1] and solid breeding blankets in fusion demonstration (DEMO) reactors.[2,3] However, the radiogenic gas tritium (hydrogen isotope, T) and helium (He) with different concentrations simultaneously produced by neutron irradiations will inevitably accumulate in Be[4] and beryllides,[5] which could induce structural damage[6] and degradation of material properties.[7,8] In particular, the retention of radioactive tritium could bring difficulties in the disposal of Be-based wastes. The retention and release of tritium and helium in neutron multiplier materials have been one of the key issues for the design and safety assessment of fusion reactors.[6] Beryllides, such as $Be_{12}Ti$, are superior to pure Be due to lower irradiation swelling[9] and smaller hydrogen (H) retention.[10]

Under irradiation, various defects, such as vacancies, could be produced. H or He atoms could be easily trapped by vacancies to form H/He–vacancy (abbreviated as H/He–V) complexes[11,12] owing to the attraction of vacancies to H or He atoms. With more H or He atoms binding to H/He–V complexes, small gas bubbles begin to form, and finally grow large with the coalescence of small bubbles.[12] The distribution, density and mean size of the He bubbles are dependent on the irradiation temperature, the structure of the irradiated material itself and the energy and concentration of the implanted He ions.[13,14] The synergistic effect between He and H atoms is an interesting topic of research in gas retention and release. It has been reported[15] that, in Be co-deposits, a lower He concentration could promote the retention of deuterium (hydrogen isotope, D) while a higher He concentration could reduce the retention of D. He bubbles could grow larger under subsequent H irradiations.[12] The evidence for the co-existence of T and He in common bubbles has been found in research on the desorption of T and He atoms in Be.[16,17] During the evolution of mixed gas bubbles, which contain both H and He atoms, H atoms tend to be distributed on the surface of the He bubbles.[18,19] However, to our knowledge, the phenomena of mixed bubbles containing both H and He atoms are rarely reported in titanium beryllide $Be_{12}Ti$.

[a]*School of Nuclear Science and Technology, Lanzhou University, Lanzhou, 730000, China. E-mail: liyuhong@lzu.edu.cn*

[b]*Institute of Modern Physics, Chinese Academy of Sciences, Lanzhou, 730000, China. E-mail: clwang@impcas.ac.cn*

[c]*School of Nuclear Science and Technology, University of Chinese Academy of Sciences, Beijing, 100049, China*

[d]*Advanced Energy Science and Technology Guangdong Laboratory, Huizhou, 516000, China*

† Contributed equally to this work.

First-principles calculations could provide a feasible way to better understand the physical micromechanism of various irradiation effects.[20–22] In particular, the early stage of nucleation of He or H bubbles has been widely simulated by first-principles calculations.[23–25] For pure Be, the calculated formation energy of a monovacancy is consistent with the data deduced from experiment.[26] Divacancies in Be are energetically unstable,[27] but He atoms could stabilize the divacancies when they bind to divacancy clusters, which are in specific orientations.[28] A monovacancy could trap up to five H atoms or twelve He atoms in pure Be, and the formation of a H_2 molecule is impossible.[29] The research[30] has shown that the diffusion of a single H atom in $Be_{12}Ti$ with a vacancy becomes relatively difficult due to a higher barrier energy compared with that in perfect $Be_{12}Ti$. This indicates that vacancies could act as traps for H atoms. It has been further investigated[31] that three different types of Be vacancies could all trap four H atoms and a Ti vacancy could trap ten H atoms.

However, few works have been focused on the investigation of the micromechanism of He bubble nucleation, especially the influence of the presence of H atoms on the He bubbles, *i.e.*, the synergistic effect of H and He atoms in $Be_{12}Ti$. The purpose of this work is to model the nucleation of He bubbles, primarily by investigating the ability of a monovacancy to trap multiple He atoms in $Be_{12}Ti$. Besides, the mixed bubbles containing both H and He atoms are also simulated further to explore the synergistic effect of H and He atoms, which is significant in understanding the micromechanism behind the retention of He and H atoms in $Be_{12}Ti$.

2 Computational methodology

In this work, all the first-principles calculations are carried out within the density functional theory (DFT) framework as implemented in the Vienna *Ab initio* Simulation Package (VASP).[32,33] The ion–electron interaction is described using the projector augmented-wave (PAW) method.[34] The generalized gradient approximation (GGA) developed by Perdew and Wang[35] has been employed to calculate the exchange–correlation energy. All the defect calculations are performed based on a tetragonal supercell containing 208 atoms. The plane-wave cutoff energy is set as 500 eV, and a *k*-point mesh of $2 \times 2 \times 4$ is employed for Brillouin-zone integration according to the Monkhorst–Pack scheme,[36] which has been well tested. The shape and volume of perfect bulk $Be_{12}Ti$ have been fully relaxed and the dimensions are kept fixed for all the defect calculations. For the geometry optimization, all atoms are relaxed until the total energy difference and forces on each atom are less than 10^{-6} eV and 0.001 eV $Å^{-1}$, respectively.

The solution energy for a single H or He atom at an interstitial site in $Be_{12}Ti$ has the following formalism:

$$E_{sol} = E(H/He) - E(bulk) - \frac{1}{2}E(H_2)/E(He) \quad (1)$$

where E(H/He) is the total energy of perfect $Be_{12}Ti$ containing one H or He atom in an interstitial site, E(bulk) is the total energy of perfect $Be_{12}Ti$, $E(H_2)$ and E(He) are the total energies of one H_2 molecule or one isolated He atom in the vacuum, respectively.

The formation energy of one vacancy in $Be_{12}Ti$ has the following formalism:

$$E_{for} = E(V) - E(bulk) + \mu_X \quad (2)$$

where E(V) is the total energy of the supercell with one vacancy, μ_X is the chemical potential of element X (X = Be, Ti).

The binding energy between one vacancy and a single H or He atom has the following formalism:

$$E_{bind} = E(H/He,V) - E(H/He) - E(V) + E(bulk) \quad (3)$$

where E(H/He,V) is the total energy of the supercell containing one vacancy and one H or He atom. A positive binding energy indicates that the interaction between the vacancy and H/He is repulsive, while it is attractive with a negative binding energy.[37]

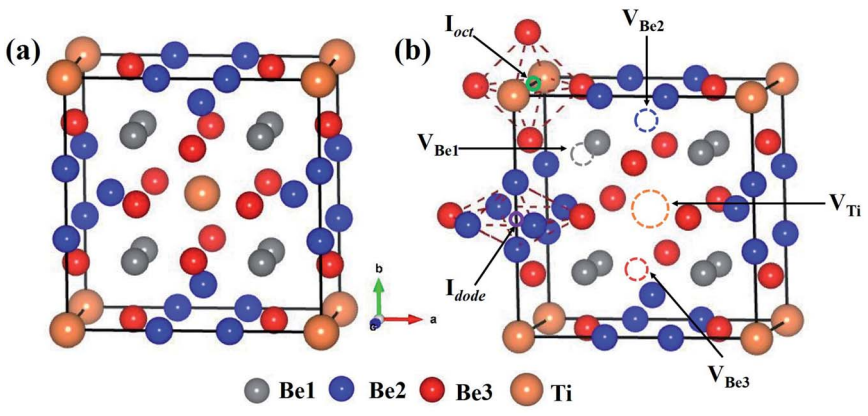

Fig. 1 (a) Schematic diagram for the unit cell of the tetragonal $Be_{12}Ti$ crystal structure, (b) schematic diagram for the four vacancies (V_{Ti}, V_{Be1}, V_{Be2} and V_{Be3}) and two interstitial sites (I_{oct} and I_{dode}) in $Be_{12}Ti$. The orange, grey, blue and red spheres denote Ti, Be1, Be2 and Be3 atoms, respectively. The orange, grey, blue and red circles represent V_{Ti}, V_{Be1}, V_{Be2} and V_{Be3}, respectively. The green and purple circles refer to I_{oct} and I_{dode}, respectively.

The solution energy for nHe and/or mH atoms ($n \geq 1$, $m \geq 0$) in $Be_{12}Ti$ with one vacancy is calculated by the following formalism:

$$E_{sol} = E(n\mathrm{He}, \mathrm{V}, m\mathrm{H}) - E(\mathrm{V}) - nE(\mathrm{He}) - \frac{m}{2}E(\mathrm{H}_2) \quad (4)$$

where E(nHe,V,mH) refers to the total energy of the system containing nHe atoms, one vacancy and/or mH atoms.

To interpret the degree of lattice deformation, the deformation energy induced by the incorporation of nHe and/or mH atoms into the system with one vacancy has also been calculated by the following formalism:

$$E_{def} = E[(\mathrm{He}_n\text{–V–H}_m)\text{–}n\mathrm{He}\text{–}m\mathrm{H}] - E(\mathrm{V}) \quad (5)$$

where E[(He_n–V–H_m)–nHe–mH] refers to the static energy of the distorted supercell after nHe and/or mH atoms have been removed. E(V) represents the static energy of the original undistorted supercell which contains one vacancy.

The trapping energy has been defined as the energy required to move an interstitial He atom into one vacancy or an interstitial H atom into a He_n–V complex. For He atoms trapped by one vacancy, the trapping energy has the following formalism:

$$E_{trap} = E(\mathrm{He}_n\text{–V})\ E(\mathrm{He}_{n-1}\text{–V}) - E(\mathrm{He_I}) + E(\mathrm{bulk}) \quad (6)$$

where E(He_n–V) represents the total energy of the supercell containing one He_n–V complex and E($\mathrm{He_I}$) corresponds to the total energy of the supercell with one He atom in an interstitial site.

For H atoms trapped by a He_n–V complex, the trapping energy has the following formalism:

$$E_{trap} = E(\mathrm{He}_n\text{–V–H}_m) - E(\mathrm{He}_n\text{–V–H}_{m-1}) - E(\mathrm{H_I}) + E(\mathrm{bulk}) \quad (7)$$

where E(He_n–V–H_m) is the total energy of the supercell containing the He_n–V–H_m complex. E($\mathrm{H_I}$) represents the total energy of the supercell containing one H atom in an interstitial site.

The bulk $Be_{12}Ti$ has tetragonal symmetry in the space group of I_4/mmm.[38,39] Ti atoms occupy the Wyckoff position of the 2a lattice site (0, 0, 0), and three symmetrically different Be atoms, which are labeled as Be1, Be2 and Be3, occupy the Wyckoff positions of 8f (0.25, 0.25, 0.25), 8i (0.361, 0, 0) and 8j (0.277, 0.5, 0), respectively. The structure of the unit cell for $Be_{12}Ti$ is shown in Fig. 1(a), where the orange spheres represent Ti atoms and the grey, blue and red spheres represent Be1, Be2 and Be3 atoms, respectively. The obtained lattice constants are $a = b = 7.328$ Å, and $c = 4.145$ Å, which are in good agreement with previous experimental[38,40] and theoretical calculation results.[31,41,42]

Table 1 Formation energies of the four different vacancies in bulk $Be_{12}Ti$

Configuration	V_{Be1} (eV)	V_{Be2} (eV)	V_{Be3} (eV)	V_{Ti} (eV)
This work	1.658	1.450	1.568	3.949
Ref. [30]	1.650	1.440	1.560	3.920
Ref. [41]	1.600	1.430	1.530	4.100

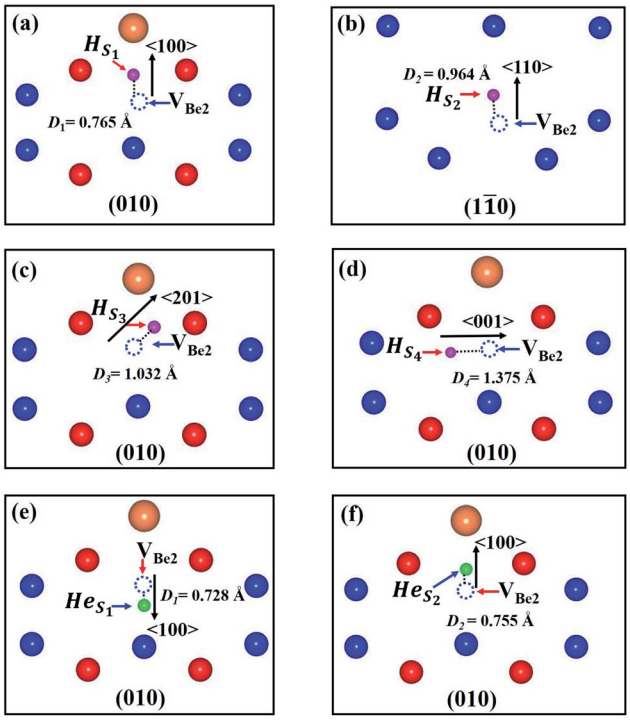

Fig. 2 (a)–(d) Four stable configurations for an individual H atom near to V_{Be2}. (e) and (f) Two stable configurations for an individual He atom near to V_{Be2}. The orange, blue, red, green and pink spheres denote Ti, Be2, Be3, He and H atoms, respectively. The blue circles represent V_{Be2}.

3 Results and discussion

3.1 Stability of individual H and He atoms in $Be_{12}Ti$

The stability of individual H and He atoms in perfect $Be_{12}Ti$ has been investigated. There are seven energetically stable interstitial sites for single H and He atoms.[30] For a single H atom, it has the lowest solution energy of 0.509 eV at an octahedral interstitial site (I_{oct}), as shown in Fig. 1(b). For an individual He atom, it preferentially occupies a dodecahedral interstitial site (I_{dode}) (Fig. 1(b)) with the lowest solution energy of 4.028 eV. These results are consistent with the previous results.[30]

There are four types of vacancies: V_{Be1} (Be1 vacancy), V_{Be2} (Be2 vacancy), V_{Be3} (Be3 vacancy) and V_{Ti} (Ti vacancy), as shown

Table 2 Solution and binding energies of individual H/He atoms at the different stable sites near to V_{Be2} in bulk $Be_{12}Ti$

Configuration	Distance (Å)	E_{sol} (eV)	E_{bind} (eV)
H_{S_1}	0.765	0.074	−0.435
H_{S_2}	0.964	−0.079	−0.588
H_{S_3}	1.032	−0.160	−0.670
H_{S_4}	1.375	0.298	−0.212
He_{S_1}	0.728	1.898	−2.130
He_{S_2}	0.755	2.236	−1.792

Table 3 Solution energies, trapping energies and deformation energies of He_n–V_{Be2} complexes ($n \leq 8$), He_n–$V_{Be2}V_{Be1}$ complexes ($n = 9$, 10, and 11) and the He_{12}–$V_{Be2}V_{Be1}V_{Be3}$ complex

Configuration	E_{sol} (eV)	E_{trap} (eV)	E_{def} (eV)
He_1–V_{Be2}	1.898	−2.130	0.191
He_2–V_{Be2}	4.402	−1.525	0.525
He_3–V_{Be2}	7.717	−0.713	1.458
He_4–V_{Be2}	10.725	−1.019	2.504
He_5–V_{Be2}	13.989	−0.764	3.602
He_6–V_{Be2}	17.167	−0.851	4.908
He_7–V_{Be2}	20.287	−0.908	6.207
He_8–V_{Be2}	23.479	−0.836	7.591
He_9–$V_{Be2}V_{Be1}$	26.040	−1.467	9.631
He_{10}–$V_{Be2}V_{Be1}$	28.594	−1.475	10.439
He_{11}–$V_{Be2}V_{Be1}$	31.545	−1.078	11.687
He_{12}–$V_{Be2}V_{Be1}V_{Be3}$	34.605	−0.968	12.936

in Fig. 1(b). The formation energies of these vacancies are summarised in Table 1, together with previous results for comparison. Obviously, the vacancy V_{Be2} has the lowest formation energy among these vacancies. Therefore, we have only investigated the interactions between the defect of V_{Be2} and H/He atoms throughout the work. A thorough search has been performed to ascertain the preferential site for both H and He atoms around V_{Be2}.

As we can see from Fig. 2, there are four stable sites and two stable sites distributed in the different crystallographic planes for the presence of single H and He atoms, respectively. Meanwhile, the solution energies and binding energies are presented in Table 2. V_{Be2} exhibits attraction to both H and He atoms. For a single H atom, V_{Be2} has the strongest attraction to a H atom, with a binding energy of −0.670 eV. H atom and V_{Be2} are distributed approximately along the direction of ⟨201⟩ in the plane of (010), and the distance between the H atom and the center of the Be2 vacancy is 1.032 Å, as shown in Fig. 2(c). For a single He atom, the configuration shown in Fig. 2(e) corresponds to the most stable state, with a binding energy of −2.130 eV and a distance of 0.728 Å. A similar tendency could also be observed for the solution energies.

3.2 Nucleation mechanism of a He bubble in the most stable monovacancy

It has been revealed that monovacancy V_{Be2} is preferentially formed in bulk $Be_{12}Ti$. It is important to get insight into the nucleation mechanism of a He bubble in V_{Be2}. Thus, the nucleation process of He_n–V_{Be2} complexes (n is the number of He atoms, $n \geq 1$) has been investigated in the following paragraph.

Considering the low He concentration, He atoms are placed near to V_{Be2} one by one, that is, the "sequential way"[43] has been

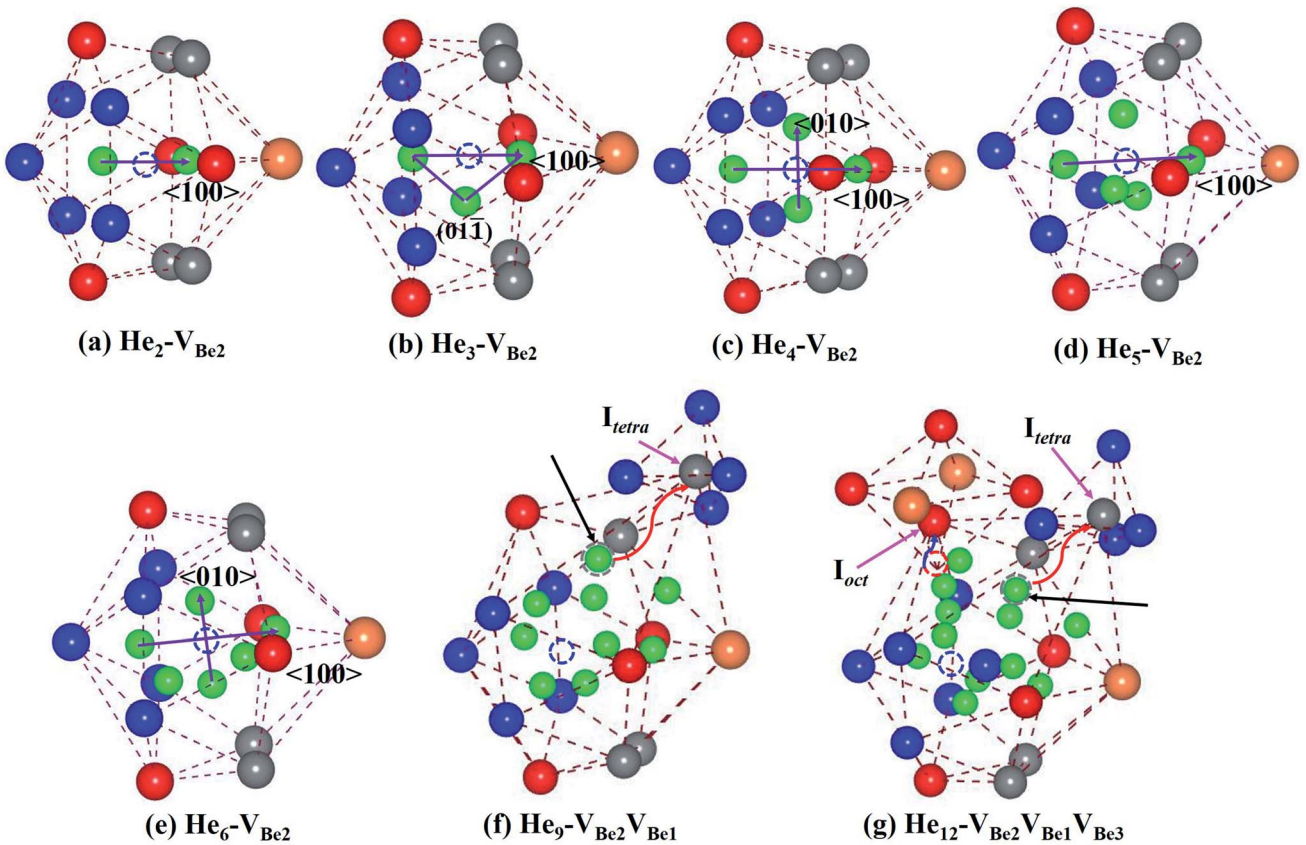

Fig. 3 The most stable configurations of the He_n–V_{Be2} complexes ($n = 2$, 3, 4, 5 and 6), the He_9–$V_{Be2}V_{Be1}$ complex and the He_{12}–$V_{Be2}V_{Be1}V_{Be3}$ complex are presented. The orange, grey, blue, red and green spheres denote Ti, Be1, Be2, Be3 and He atoms, respectively. The grey, blue and red circles refer to Be1, Be2 and Be3 vacancies, respectively.

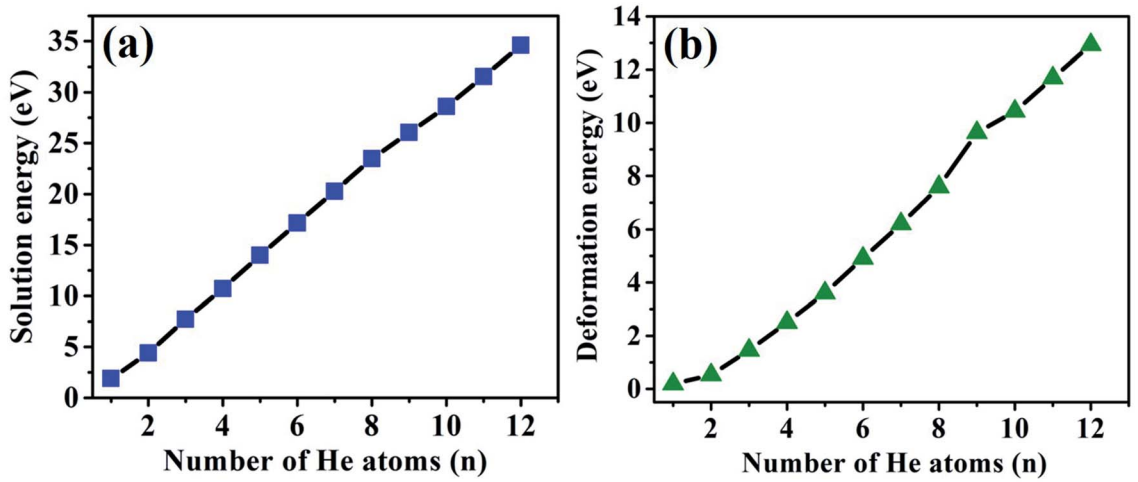

Fig. 4 The relationship of solution energies and deformation energies of the He_n–V_{Be2} ($n \leq 8$), He_n–$V_{Be2}V_{Be1}$ (n = 9, 10, and 11) and He_{12}–$V_{Be2}V_{Be1}V_{Be3}$ complexes with the number of implanted He atoms.

adopted to simulate the nucleation of the He bubble; this has also been applied in many investigations related to the nucleation of He or H bubbles.[44,45] The solution energies, trapping energies and deformation energies are summarised in Table 3. For the simplest He–V_{Be2} complex, the most stable configuration has been obtained, as shown in Fig. 2(e). When an extra He atom is trapped by a He–V_{Be2} complex, the He_2–V_{Be2} complex has the configuration of a dumbbell with a trapping energy of −1.525 eV, which exactly distributes along the direction of ⟨100⟩, as shown in Fig. 3(a). The distance between two He atoms is 1.611 Å, and V_{Be2} is located in the middle of the dumbbell. When the third He atom is implanted into the He_2–V_{Be2} complex, the above mentioned dumbbell configuration is also observed, but the distance between the two He atoms increases to 1.976 Å. The distances between the third He atom and the other two He atoms are 1.499 Å and 1.524 Å. Thus, the He_3–V_{Be2} complex has the approximate shape of an isosceles triangle located in the plane of $(01\bar{1})$, which is shown in Fig. 3(b). The trapping energy of the He atoms is −0.713 eV. In the He_4–V_{Be2} complex with a trapping energy of −1.019 eV, as shown in Fig. 3(c), besides the dumbbell distributing along the direction of ⟨100⟩, another dumbbell configuration is also observed, which distributes along the direction of ⟨010⟩. In the most stable configuration of the He_5–V_{Be2} complex with a trapping energy of −0.764 eV, the initial dumbbell slightly deviates from its original direction of ⟨100⟩. Whereas the dumbbell with a direction of ⟨010⟩ disappears, as shown in Fig. 3(d). In the configuration of the He_6–V_{Be2} complex, there are also two dumbbells: one approximately distributes along the direction of ⟨100⟩, and the other is along the direction of $\langle 01\bar{1}\rangle$, as shown in Fig. 3(e). The trapping energy of the He atoms is −0.851 eV. In the most stable configuration of the He_7–V_{Be2} complex, dumbbells similar to those in the He_4–V_{Be2} complex are also obtained. The trapping energy for the He atoms is −0.908 eV. When one new He atom is added into the He_7–V_{Be2} complex, the two dumbbells deviate from their original directions. The trapping energy of the He atoms is −0.836 eV. The deformation of the lattice becomes more obvious, where some of Be atoms near the He_8–V_{Be2} complex begin to deviate from their lattice sites due to the repulsion of He atoms.

Things become more interesting once the most stable configuration of the He_9–V_{Be2} complex has been formed. As we

Table 4 Solution energies, trapping energies and deformation energies for the He_n–V_{Be2}–H_m ($n \leq 6$, $m \leq 6$) complexes

Configuration	E_{sol} (eV)	E_{trap} (eV)	E_{def} (eV)
He_1–V_{Be2}–H_1	1.827	−0.580	0.261
He_1–V_{Be2}–H_2	1.933	−0.403	0.362
He_1–V_{Be2}–H_3	2.352	−0.091	0.568
He_1–V_{Be2}–H_4	2.840	−0.021	0.727
He_1–V_{Be2}–H_5	3.401	0.053	1.131
He_2–V_{Be2}–H_1	4.711	−0.200	0.720
He_2–V_{Be2}–H_2	5.053	−0.168	0.891
He_2–V_{Be2}–H_3	5.540	−0.022	1.122
He_2–V_{Be2}–H_4	6.044	−0.005	1.345
He_2–V_{Be2}–H_5	6.637	0.084	1.670
He_3–V_{Be2}–H_1	7.973	−0.253	1.712
He_3–V_{Be2}–H_2	8.253	−0.230	1.904
He_3–V_{Be2}–H_3	8.662	−0.100	2.174
He_3–V_{Be2}–H_4	9.144	−0.026	2.549
He_3–V_{Be2}–H_5	9.704	0.051	2.841
He_4–V_{Be2}–H_1	10.960	−0.274	2.816
He_4–V_{Be2}–H_2	11.233	−0.237	3.068
He_4–V_{Be2}–H_3	11.670	−0.073	3.427
He_4–V_{Be2}–H_4	12.181	0.002	3.814
He_5–V_{Be2}–H_1	14.211	−0.287	3.902
He_5–V_{Be2}–H_2	14.501	−0.219	4.267
He_5–V_{Be2}–H_3	14.902	−0.109	4.678
He_5–V_{Be2}–H_4	15.373	−0.038	4.955
He_5–V_{Be2}–H_5	15.929	0.047	5.432
He_6–V_{Be2}–H_1	17.406	−0.270	5.218
He_6–V_{Be2}–H_2	17.742	−0.173	5.651
He_6–V_{Be2}–H_3	18.199	−0.052	5.987
He_6–V_{Be2}–H_4	18.674	−0.034	6.343
He_6–V_{Be2}–H_5	19.176	−0.007	7.164
He_6–V_{Be2}–H_6	19.807	0.122	7.390

can see from Fig. 3(f), one Be1 atom near V_{Be2} is completely pushed out from its lattice site into a tetrahedral interstitial site (I_{tetra}). The newly produced vacancy, V_{Be1}, is occupied by one He atom. The trapping energy drops dramatically to −1.467 eV. Next, the He_n–$V_{Be2}V_{Be1}$ complexes ($n \geq 9$) will nucleate around V_{Be2} and V_{Be1}. And V_{Be1} is occupied by one He atom. In particular, in the He_{12}–$V_{Be2}V_{Be1}$ complex, a similar phenomenon can also be observed that one Be3 atom near to V_{Be2} is exactly pushed out from its lattice site. Therefore, a new vacancy, V_{Be3}, is also induced without the occupation of a He atom. It is inferred that the He_n–$V_{Be2}V_{Be1}V_{Be3}$ complexes ($n \geq 12$) will nucleate around the three vacancies V_{Be2}, V_{Be1} and V_{Be3}. The critical configurations for the divacancy of the He_n–$V_{Be2}V_{Be1}$ complexes and the trivacany of the He_n–$V_{Be2}V_{Be1}V_{Be3}$ complexes have been obtained.

The solution and deformation energies increase approximately linearly with the sequential implantation of He atoms in the He_n–V_{Be2} complexes ($n \leq 12$), as shown in Fig. 4(a) and (b), indicating that the distortion of lattice becomes more serious as more He atoms are embedded into $Be_{12}Ti$. As we can see from Table 3, in the initial stage of He bubble nucleation, it is difficult for saturation to occur and for a positive trapping energy to be obtained. It is proposed that individual He atoms could bind to V_{Be2} and form a He–V_{Be2} complex due to the attraction of V_{Be2}. The subsequent He atoms are trapped by V_{Be2} and the He_n–V_{Be2} complexes are formed. As more He atoms are implanted, new vacancies can be produced and the capacity for He atoms can be enhanced. Thus, more He atoms can be trapped by vacancies, forming the He_n–V_i complexes (i represents the number of vacancies). Finally, He bubbles could nucleate and grow gradually.

3.3 Influence of the presence of H atoms on the nucleation of He bubbles and the trapping ability of monovacancies to H and He atoms

To explore the influence of the presence of H atoms on the nucleation of He bubbles, the capture behavior of H atoms in the He_n–V_{Be2} complexes ($n \leq 6$), *i.e.*, the synergistic effect of the H and He atoms, has been exhaustively investigated in the following paragraph. The solution energies, trapping energies, deformation energies and parts of the most stable

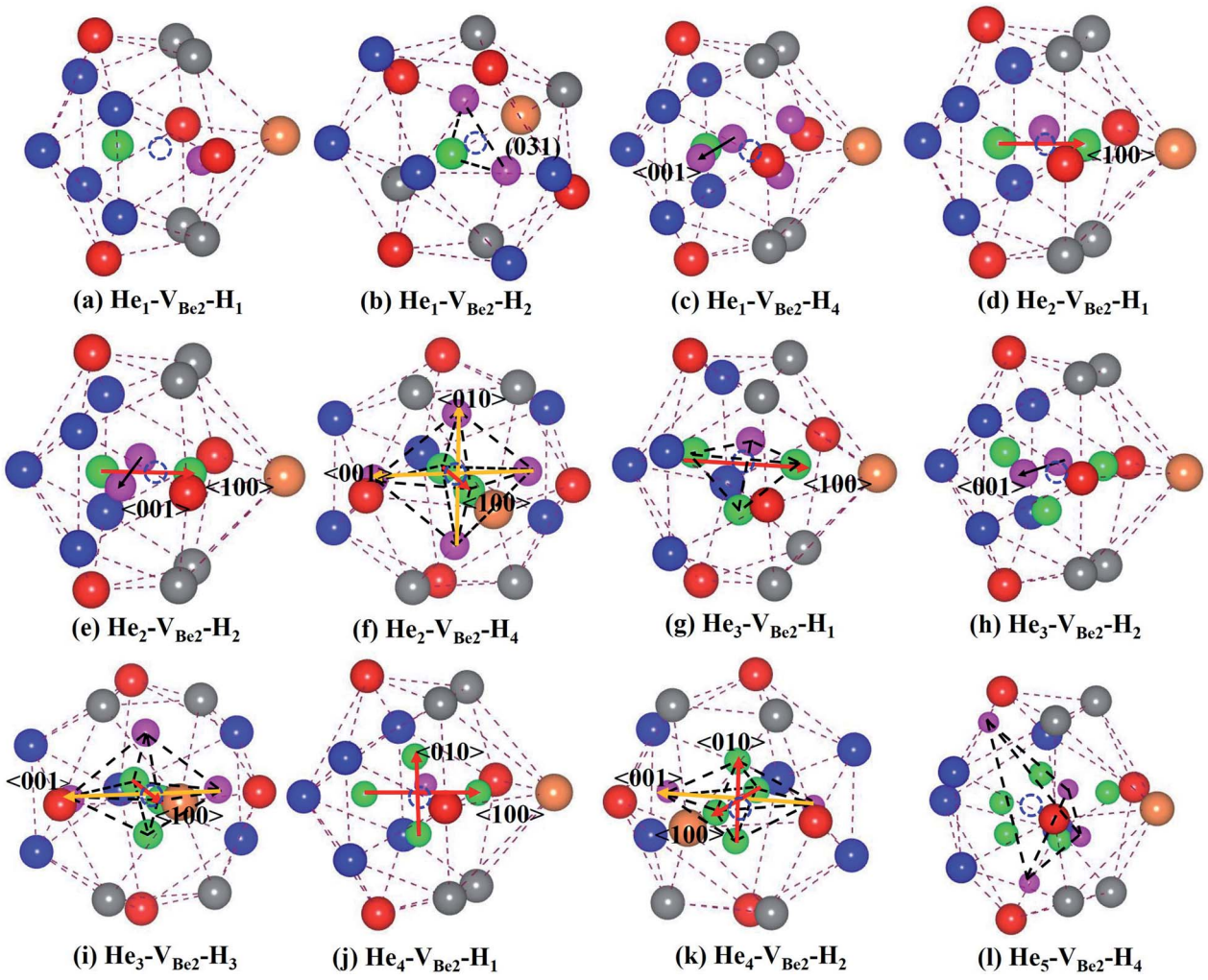

Fig. 5 Parts of the most stable configurations of the He_n–V_{Be2}–H_m complexes ($n \leq 6$). The orange, grey, blue, red, green and pink spheres denote Ti, Be1, Be2, Be3, He, and H atoms, respectively. The blue circles refer to V_{Be2}.

configurations of the He_n–V_{Be2}–H_m complexes (m is the number of H atoms) have been shown in Table 4 and Fig. 5, respectively.

As we can see from Fig. 5, in the He_1–V_{Be2}–H_1 complex, the distance between the H atom and He atom is 1.733 Å. In the most stable configuration of the He_1–V_{Be2}–H_2 complex, the two H atoms, the He atom and V_{Be2} are located in the same plane of (031). The two H atoms and the He atom form the structure of an isosceles triangle, where the distances between the He atom and each H atom are 1.773 Å. In the configuration of the He_1–V_{Be2}–H_4 complex, there are two H atoms distributed along the direction of ⟨001⟩. When another H atom is trapped by the He_1–V_{Be2}–H_4 complex, the trapping energy becomes positive, implying that the He_1–V_{Be2} complex could accommodate four H atoms at most.

In the He_2–V_{Be2}–H_1 complex, the above mentioned dumbbell distributing along the direction of ⟨100⟩ still exists. However, the distance between two He atoms is 1.648 Å, which is larger than that in the He_2–V_{Be2} complex (1.611 Å). In the He_2–V_{Be2}–H_2 complex, two H atoms also distribute along the direction of ⟨001⟩. Besides, two He atoms and two H atoms are located in the same plane of (010). In the He_2–V_{Be2}–H_4 complex, one new dumbbell structure along the direction of ⟨010⟩, which is composed of two H atoms and one V_{Be2}, could obviously be observed. Meanwhile, four H atoms and two He atoms form the structure of an octahedron. The maximal trapping ability of the He_2–V_{Be2} complex for H atoms is four.

The dumbbell distributing along the direction of ⟨100⟩ has been also observed in the He_3–V_{Be2}–H_1 complex. Four atoms (one H atom and three He atoms) form the structure of a tetrahedron. In the He_3–V_{Be2}–H_2 complex, two H atoms also distribute along the direction of ⟨001⟩. In the configuration of the He_3–V_{Be2}–H_3 complex, three H atoms and three He atoms form the structure of an octahedron. It is found that the He_3–V_{Be2} complex could also trap four H atoms.

The He_4–V_{Be2} complex could trap three H atoms at most. The two dumbbells observed in the He_4–V_{Be2} complex still exist. The structure of an octahedron, which is composed of two H atoms and four He atoms in the He_4–V_{Be2}–H_2 complex, has been obviously observed.

In the He_5–V_{Be2}–H_2 complex, two H atoms are no longer along the direction of ⟨001⟩. In the He_5–V_{Be2}–H_3 complex, the dumbbell structure along the direction of ⟨100⟩ disappears. In the He_5–V_{Be2}–H_4 complex, four H atoms form the structure of a tetrahedron. The He_5–V_{Be2} complex could also trap four H atoms. However, the He_6–V_{Be2} complex could trap up to five H atoms. Interestingly, in all the He_n–V_{Be2}–H_m complexes ($n \leq 6$, $m \leq 6$), the He atoms are located in the core surrounding V_{Be2}, while the H atoms are distributed on the surface of the core, forming a shell. This phenomenon has also been observed in W[19] and Fe.[46]

It can be seen from Fig. 6(a) and (b) that the solution energies and deformation energies of the He and H atoms in the He_n–V_{Be2}–H_m complexes ($n \leq 6$, $m \leq 6$) approximately linearly increase with the increase in the number of implanted He and H atoms, meaning that the degree of deformation increases with the sequential implantation of He and H atoms. The largest deformation will be induced by the He_6–V_{Be2}–H_m complexes. As we can see from Fig. 6(c), the He_2–V_{Be2}–H_m complexes have the maximal trapping energy. Besides, the trapping energy of all configurations will become positive when more than four H atoms are implanted around the He_n–V_{Be2} complexes. It is inferred that, in terms of their ability to trap H atoms, the He_n–V_{Be2} complexes will be saturated. The positive trapping energy means that it is difficult for the He_n–V_{Be2} complexes to trap H atoms, and the retention of H atoms will occur far away from the He_n–V_{Be2}–H_m complexes. Besides, throughout the simulation of nucleation of He_n–V_{Be2}–H_m complexes, no molecular H_2 has been observed. The distances between any arbitrary two H atoms are larger than the bond

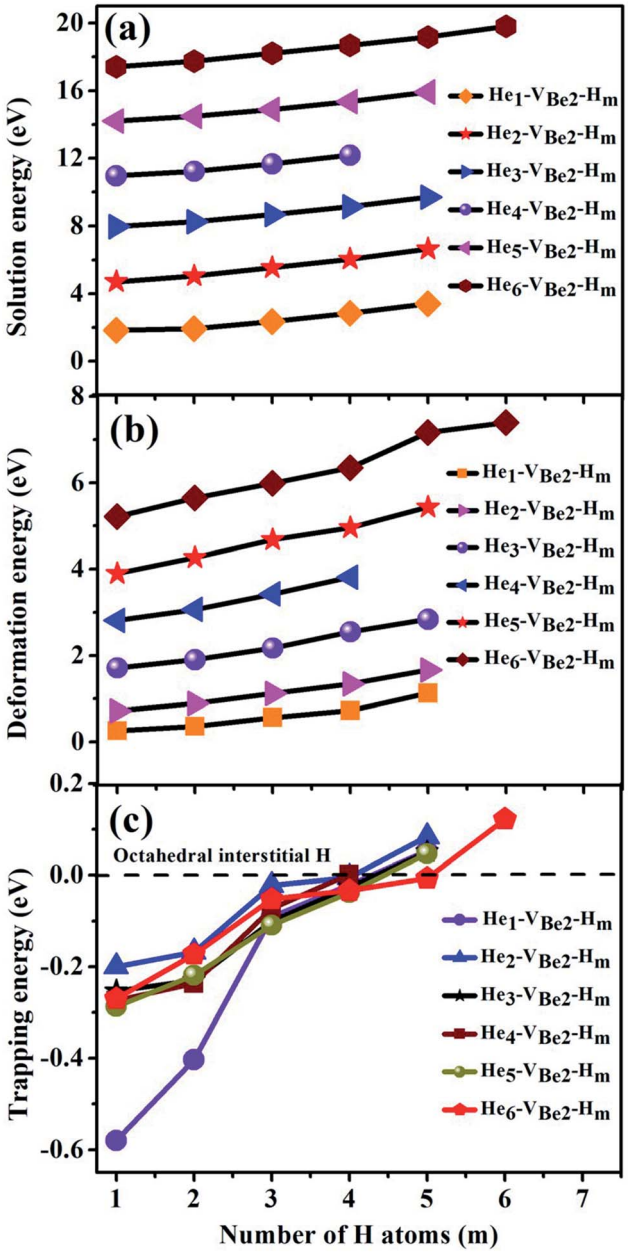

Fig. 6 Relationship of (a) solution energies, (b) deformation energies and (c) trapping energies of the He_n–V_{Be2} complexes ($n \leq 6$) with the number of implanted H atoms.

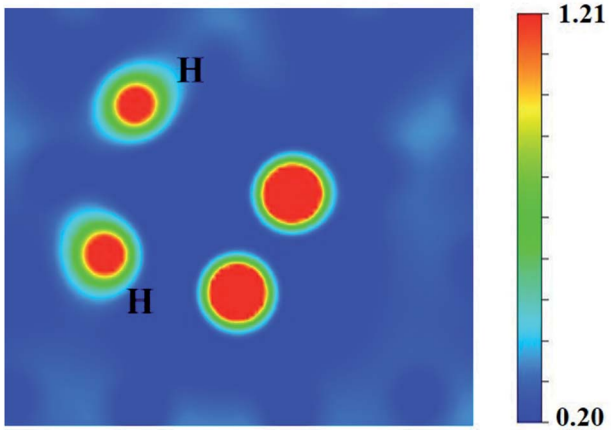

Fig. 7 The charge density (e Å^{-3}) between the two H atoms separated by a distance of 2.318 Å in the He_6–V_{Be2}–H_5 system.

length of molecular H_2, 0.74 Å. Furthermore, it has also shown that the charge density between an arbitrary two H atoms is very low. The results indicate that the interaction between the arbitrary two H atoms is very weak, and the bond of molecular H_2 cannot form. For example, in the He_6–V_{Be2}–H_5 system, the minimal distance between two H atoms is 2.318 Å, which is larger than the bond length of molecular H_2. On the other hand, as one can see from Fig. 7, the charge density between the two H atoms with a minimal distance between them of 2.318 Å is very low, which further indicates that no molecular H_2 has formed.

To better understand the mechanism for the trapping of H atoms by He_n–V_{Be2} complexes, the electronic structures of the He_1–V_{Be2}–H_m complexes have been calculated. As shown in Fig. 8, the purple curved surfaces represent the isosurface of charge density of 0.13 e Å^{-3}. The individual He atom could not fill up the charge density hole. The surface of optimal electron density gradually shrinks as H atoms are sequentially implanted into the He_1–V_{Be2} complex. When more than four H atoms are implanted, there is not enough isosurface for H atoms to combine with the complex. The residual H atoms would escape the complex due to the repulsion from other H atoms and will be trapped by other vacancies and complexes.

It has been firmly confirmed that beryllides are superior to pure Be in irradiation resistance.[9,10] Therefore, alloying is an effective method not only for inhibiting the irradiation damage, but also improving the mechanical and thermodynamic properties of materials. Ternary or more complex beryllides may be more excellent as neutron multiplier materials. Besides, in experiment, researchers could develop new techniques to fabricate beryllides which have nanoscale grains. In the materials with small grains, there will be a large fraction of interfaces and grain boundaries,[14] which also act as traps for the segregation and aggregation of transmutation-produced He and H atoms. As such, the concentrations of He and H atoms inside the grain will be relatively reduced. The irradiation induced swelling and damage could be well mitigated.

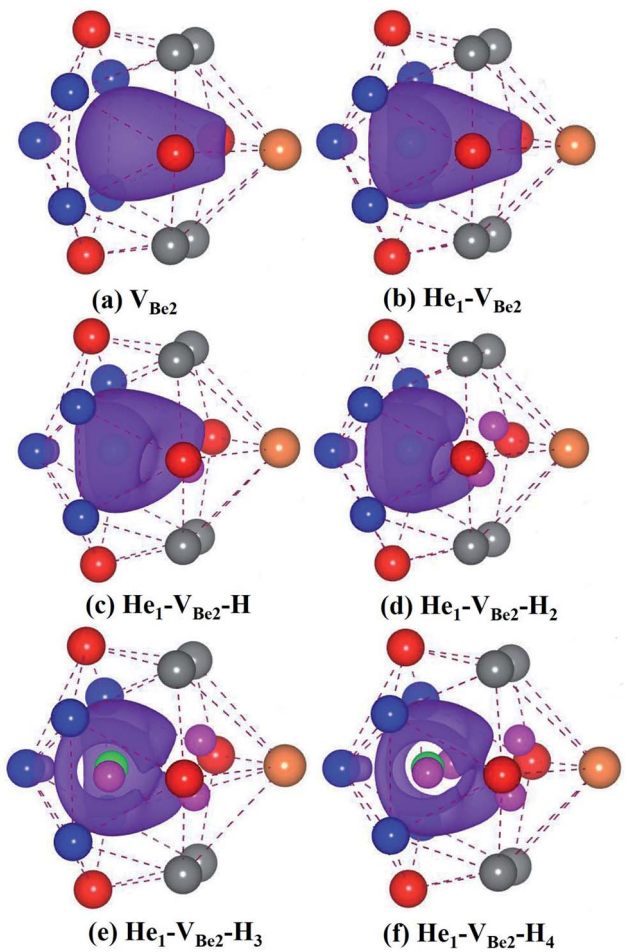

Fig. 8 Isosurfaces of charge density at the (a) V_{Be2}, (b) He_1–V_{Be2} and (c)–(f) He_1–V_{Be2}–H_m complexes (m = 1, 2, 3, and 4). The orange, grey, blue, red, green and pink spheres denote Ti, Be1, Be2, Be3, He, and H atoms, respectively. The purple curved surfaces represent the isosurface of charge density of 0.13 e Å^{-3}.

4 Conclusions

A systematic investigation has been performed to clarify the nucleation mechanism of a He bubble around a Be vacancy in bulk $Be_{12}Ti$. The influence of the presence of H atoms on the nucleation of the He bubble, *i.e.*, the synergistic effect of He and H atoms, has been further investigated. During the process of He bubble nucleation, dumbbell structures evolve with the number of implanted He atoms and finally disappear. In the He_n–V_{Be2} complexes ($n \leq 8$), the nucleation of the He bubble is around a V_{Be2} monovacancy. It becomes interesting when another He atom is embedded into the He_8–V_{Be2} complex. One new vacancy is induced and is occupied by one He atom in the He_9–V_{Be2} complex. The subsequent He bubble nucleation is around the divacancy of $V_{Be2}V_{Be1}$. When an extra He atom is implanted into the He_{11}–$V_{Be2}V_{Be1}$ complex, another new vacancy V_{Be3} is produced, but without the occupation of a He atom. It is inferred that the nucleation of the He bubble will be around the trivacancy of $V_{Be2}V_{Be1}V_{Be3}$. It is difficult to get to saturation of trapped He atoms.

In the study of the synergistic effect of He and H atoms, the implantation of H atoms into the He_n–V_{Be2} ($n \leq 6$) complexes could influence the stability of existing dumbbells. On the other

hand, some tetrahedral and octahedral structures are also obtained. The He_n–V_{Be2} ($n \leq 6$) complexes could trap approximately four H atoms. The residual H atoms could not be accommodated due to the continuous shrinking of the isosurface of charge density, but could be trapped by other vacancies or complexes far away from the He_n–V_{Be2}–H_4 ($n \leq 6$) complex. This simulation study provides a foundation to understand the evolution of the He bubble microstructure and the synergistic effect between He and H atoms in $Be_{12}Ti$, which is favorable for better understanding the retention of irradiation-induced He and H atoms in neutron multiplying materials. This investigation could be helpful for the design and fabrication of more promising beryllides which could withstand a severe external environment.

Conflicts of interest

There are no conflicts to declare.

Acknowledgements

This work is supported by the National Nature Science Foundation of China (Grant No. 11775102), the Strategic Priority Research Program of Chinese Academy of Sciences (Grant No. XDA21010202) and the Advanced Energy Science and Technology Guangdong Laboratory.

References

1 J. H. Kim and M. Nakamichi, *J. Nucl. Mater.*, 2019, **519**, 182–187.
2 D. V. Bachurin and P. V. Vladimirov, *Intermetallics*, 2018, **100**, 163–170.
3 S. C. Middleburgh and R. W. Grimes, *Acta Mater.*, 2011, **59**, 7095–7103.
4 P. Vladimirov, C. Ferrero, V. Chakin, P. Kurinskiy, A. Moeslang, R. Pieritz, T. Weitkamp and E. Brun, *Acta Mater.*, 2015, **88**, 293–301.
5 V. Chakin, R. Rolli, R. Gaisin, U. H. Kramar, M. Nakamichi and M. Zmitko, *Fusion Eng. Des.*, 2020, **161**, 111938.
6 V. Chakin, R. Rolli, A. Moeslang, M. Klimenkov, M. Kolb, P. Vladimirov, P. Kurinskiy, H. C. Schneider, S. van Til, A. J. Magielsen and M. Zmitko, *J. Nucl. Mater.*, 2013, **442**, S483–S489.
7 V. Chakin, R. Rolli, A. Moeslang, P. Vladimirov, P. Kurinskiy, S. van Til, A. J. Magielsen and M. Zmitko, *Fusion Eng. Des.*, 2013, **88**, 2309–2313.
8 V. Chakin, J. Reimann, A. Moeslang, R. Latypov and A. Obukhov, *Prog. Nucl. Energy*, 2012, **57**, 2–7.
9 K. Tsuchiya, T. Hoshino, H. Kawamura, Y. Mishima, N. Yoshida, T. Terai, S. Tanaka, K. Munakata, S. Kato, M. Uchida, M. Nakamichi, H. Yamada, D. Yamaki and K. Hayashi, *Nucl. Fusion*, 2007, **47**, 1300–1306.
10 Y. Fujii, M. Miyamoto, J. H. Kim, M. Nakamichi, N. Murayoshi and H. Iwakiri, *Nucl. Mater. Energy*, 2016, **9**, 233–236.
11 S. Y. Binyukova, I. I. Chernov, B. A. Kalin and T. Swe, *J. Nucl. Mater.*, 2007, **367–370**, 500–504.
12 W. H. Hu, L. P. Guo, J. H. Chen, F. F. Luo, T. C. Li, Y. Y. Ren, J. P. Suo and F. Yang, *Fusion Eng. Des.*, 2014, **89**, 324–328.
13 S. J. Leclerc, M. L. Lescoat, F. Fortuna, L. Legras, X. Li and A. Gentils, *J. Nucl. Mater.*, 2015, **466**, 646–652.
14 X. Y. Sun, F. D. Chen, H. Huang, J. W. Lin and X. B. Tang, *Appl. Surf. Sci.*, 2019, **467–468**, 1134–1139.
15 A. Založnik, M. J. Baldwin, R. P. Doerner, T. S. Selinger and S. Brezinsek, *J. Nucl. Mater.*, 2018, **512**, 25–30.
16 I. B. Kupriyanov, G. N. Nikolaev, V. V. Vlasov, A. M. Kovalev and V. P. Chakin, *J. Nucl. Mater.*, 2007, **367–370**, 511–515.
17 E. Rabaglino, J. P. Hiernaut, C. Ronchi and F. S. Argentina, *J. Nucl. Mater.*, 2002, **307–311**, 1424–1429.
18 E. Abramov and D. Eliezer, *J. Mater. Sci.*, 1992, **27**, 2595–2598.
19 N. Juslin and B. D. Wirth, *J. Nucl. Mater.*, 2013, **438**, S1221–S1223.
20 W. A. Counts, C. Wolverton and R. Gibala, *Acta Mater.*, 2010, **58**, 4730–4741.
21 P. B. Zhang, J. J. Zhao and B. Wen, *J. Nucl. Mater.*, 2012, **429**, 216–220.
22 H. F. Zhang, B. D. Yao, L. Q. Shi, D. J. O'Connor, J. Huang, J. Y. Zhang, W. Ding and Y. X. Wang, *Acta Mater.*, 2015, **97**, 50–57.
23 Z. C. Meng, C. L. Wang, J. T. Liu, Y. L. Wang, X. L. Zhu, L. Yang and L. Huang, *Phys. Chem. Chem. Phys.*, 2020, **22**, 18040–18049.
24 Y. G. Xu, X. J. Bai, X. H. Zha, Q. Huang, J. He, K. Luo, Y. H. Zhou, T. C. Germann, J. S. Francisco and S. Y. Du, *J. Chem. Phys.*, 2015, **143**, 114707.
25 J. J. Liu, C. L. Wang, X. L. Zhu, J. T. Liu, X. M. Zhang, X. Q. Gou, W. S. Duan and L. Yang, *Phys. Chem. Chem. Phys.*, 2018, **20**, 18766–18774.
26 L. Ferry, F. Virot, M. Barrachin, Y. Ferro, C. Pardanaud, D. Matveev, M. Wensing, T. Dittmar, M. Koppen and C. Linsmeier, *Nucl. Mater. Energy*, 2017, **12**, 453–457.
27 M. G. Ganchenkova and V. A. Borodin, *Phys. Rev. B: Condens. Matter Mater. Phys.*, 2007, **75**, 054108.
28 P. V. Vladimirov and A. Moeslang, *J. Nucl. Mater.*, 2013, **442**, S694–S698.
29 P. B. Zhang, J. J. Zhao and B. Wen, *J. Phys.: Condens. Matter*, 2012, **24**, 095004.
30 X. L. Zhu, C. L. Wang, J. J. Liu, X. M. Zhang, H. Q. Deng, W. S. Duan and L. Yang, *RSC Adv.*, 2018, **8**, 35735.
31 X. L. Zhu, C. L. Wang, Z. C. Meng, Y. L. Wang, H. Q. Deng, W. S. Duan and L. Yang, *J. Nucl. Mater.*, 2019, **525**, 7–13.
32 G. Kresse and J. Furthmüller, *Phys. Rev. B: Condens. Matter Mater. Phys.*, 1996, **54**, 11169–11186.
33 G. Kresse and J. Furthmüller, *Comput. Mater. Sci.*, 1996, **6**, 15–50.
34 P. E. Blöchl, *Phys. Rev. B: Condens. Matter Mater. Phys.*, 1994, **50**, 17953–17979.
35 J. P. Perdew and Y. Wang, *Phys. Rev. B: Condens. Matter Mater. Phys.*, 1992, **45**, 13244.
36 H. J. Monkhorst and J. D. Pack, *Phys. Rev. B: Solid State*, 1976, **13**, 5188–5192.

37 Q. Zhao, Z. Zhang, M. Huang, X. D. Zhang and X. P. Ouyang, *Nucl. Instrum. Methods Phys. Res., Sect. B*, 2020, **470**, 48–55.
38 E. Gillam, H. P. Rooksby and L. D. Brownlee, *Acta Crystallogr.*, 1964, **17**, 762–763.
39 M. L. Jackson, P. A. Burr and R. W. Grimes, *Acta Crystallogr., Sect. B: Struct. Sci., Cryst. Eng. Mater.*, 2016, **B72**, 277–280.
40 A. Zalkin, D. E. Sands, R. G. Bedford and O. H. Krikorian, *Acta Crystallogr.*, 1961, **14**, 63–65.
41 M. L. Jackson, P. A. Burr and R. W. Grimes, *Nucl. Fusion*, 2017, **57**, 086049.
42 X. K. Liu, Q. J. Feng, B. Tang, J. Zheng, Z. Zheng, W. Zhou, J. T. Tian and J. Wang, *RSC Adv.*, 2019, **9**, 5302.
43 A. Alkhamees, H. B. Zhou, Y. L. Liu, S. Jin, Y. Zhang and G. H. Lu, *J. Nucl. Mater.*, 2013, **437**, 6–10.
44 M. A. Tschopp, F. Gao and K. N. Solanki, *Acta Mater.*, 2017, **124**, 544–555.
45 W. Counts, C. Wolverton and R. Gibala, *Acta Mater.*, 2011, **59**, 5812–5820.
46 E. Hayward and C. Deo, *J. Phys.: Condens. Matter*, 2012, **24**, 265402.